

## Double Gyroid Network Morphology in Supramolecular Diblock Copolymer Complexes

Ivana Vukovic,<sup>†</sup> Thomas P. Voortman,<sup>†</sup> Daniel Hermida Merino,<sup>‡</sup> Giuseppe Portale,<sup>‡</sup> Panu Hiekkataipale,<sup>§</sup> Janne Ruokolainen,<sup>§</sup> Gerrit ten Brinke,<sup>\*,†</sup> and Katja Loos<sup>\*,†</sup>

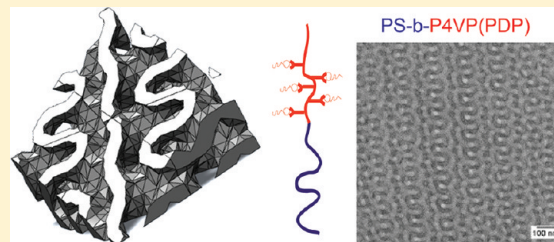
<sup>†</sup>Department of Polymer Chemistry, Zernike Institute for Advanced Materials, University of Groningen, Nijenborgh 4, 9747 AG Groningen, The Netherlands

<sup>‡</sup>Netherlands Organization for Scientific Research, DUBBLE beamline at the ESRF, 6 rue Jules Horowitz, BP 220, 38043, CEDEX 9, Grenoble, France, and Dutch Polymer Institute

<sup>§</sup>Molecular Materials, Department of Applied Physics, Aalto University (formerly Helsinki University of Technology), Puumiehenkuja 2, 02015 Espoo, Finland

### S Supporting Information

**ABSTRACT:** The double gyroid network morphology has been the focus of extensive research efforts as one of the most appealing block copolymer structures for practical applications. We performed an extensive study of the phase behavior of the supramolecular complex PS-*b*-P4VP(PDP)<sub>x</sub> to develop a systematic route to its double gyroid morphology. The morphological characterization of complexes was accomplished by transmission electron microscopy (TEM) and small-angle X-ray scattering (SAXS). Several compositions with the cubic *Ia*3d symmetry were found in a narrow region between the lamellar and the cylindrical phase. Experimental TEM images were compared to computer simulations of projections through multiple gyroid planes. Typical gyroid patterns—“double wave” and “wagon wheel”—were regularly found. The size of the gyroid unit cell was calculated from the SAXS data. The lattice parameter could be varied (from ca. 70 to 125 nm) by altering the molar mass of the block copolymer precursors. A number of complexes were found to exhibit characteristic biphasic morphologies—coexisting lamellar and gyroid phase or gyroid and cylindrical phase. Finally, gyroid complexes with different relative PDP ratios were obtained which provides the opportunity to generate nanoporous structures with tunable porosities by dissolving the amphiphiles.



### INTRODUCTION

Self-assembly in block copolymers has attracted a lot of attention since the development of living anionic polymerization<sup>1</sup> and the subsequent experimental discovery of ordered mesostructures in the simplest linear AB diblock copolymers.<sup>2–6</sup> More complex systems such as triblock and multiblock copolymers, star-type and graft-type copolymers, blends of block copolymers with homopolymers, etc., are found to exhibit a broad variety of novel morphologies.<sup>7–13</sup>

The bicontinuous gyroid morphology has captivated researchers due to a wide range of possible technological applications, such as hybrid solar cells,<sup>14</sup> antireflection structures,<sup>15</sup> photonic crystals,<sup>16</sup> optical metamaterials,<sup>17</sup> etc. In comparison to classical phases (body-centered cubic spheres (BCC), hexagonally ordered cylinders (CYL), and lamellae (LAM)), a bicontinuous gyroid morphology appears over a narrow range of the copolymer composition *f* in the diblock copolymer phase diagram. It is mostly found in the weak-to-intermediate segregation regime ( $10 < \chi N < 40$ ), and its region in the phase diagram gradually contracts as  $\chi N$  increases, possibly due to the packing frustration induced by narrowing interfaces in the strong segregation regime.<sup>18</sup> Therefore, careful selection of the block copolymer system parameters is required to target the gyroid region of the phase diagram. Another

challenge that is of crucial importance for certain applications is the ability to control the domain size in the gyroid unit cell. For instance, interdomain spacing of several hundreds of nanometers is required for a visible-light photonic crystal<sup>16</sup> while it should be comparable to the exciton diffusion length ( $\sim 10$  nm) for a hybrid solar cell application.<sup>14</sup>

Addition of another component to a block copolymer alters its phase behavior and can affect the appearance of new equilibrium morphologies, particularly between LAM and CYL phases.<sup>19–21</sup> Studies of the phase behavior of diblock copolymer/homopolymer blends have shown that bicontinuous phases can be stabilized by the presence of the homopolymer.<sup>22,23</sup> Another example is the appearance of the core–shell double gyroid morphology when the amphiphilic molecule PDP (pentadecylphenol) is added to the triblock copolymer PtBOS-*b*-PS-*b*-P4VP (poly(*tert*-butoxystyrene)-*b*-polystyrene-*b*-poly(4-vinylpyridine)).<sup>24</sup> Moreover, it is possible to tailor the morphology of the system in a simple fashion by varying the relative fraction of the additional component and thus saving the effort of

Received: February 9, 2012

Revised: March 28, 2012

Published: April 6, 2012

synthesizing a block copolymer to achieve the desired morphology.<sup>25</sup>

The focus of this study is the formation of the double gyroid network morphology in supramolecular complexes of amphiphilic PDP and PS-*b*-P4VP (polystyrene-*b*-poly(4-vinylpyridine)) diblock copolymers. PDP molecules interact via hydrogen bonds with pyridine rings to form PS-*b*-P4VP(PDP)<sub>x</sub> complexes (*x* denotes the ratio between PDP molecules and P4VP repeat units). The amphiphiles can be removed in a selective solvent to generate nanoporous structures.<sup>26,27</sup> If the nanoporous material has a continuous morphology, the critical alignment issue is overcome which provides the opportunity for several applications, such as membranes,<sup>28</sup> templates for inorganic materials, etc.<sup>14,15,17,29,30</sup> In our previous work we showed that gyroid PS-*b*-P4VP(PDP)<sub>x</sub> complexes can be exploited as precursors for well-ordered metal nanofoams.<sup>31</sup>

In the study of the phase diagram of the PS-*b*-P4VP(PDP)<sub>1.0</sub> complex, Valkama et al. have reported the formation of the double gyroid morphology in a sample with the weight fraction of PS ( $f_{PS}$ ) 0.38 and the total molar mass (including PDP) 83 300 g mol<sup>-1</sup>. When the total molar mass was increased to 129 000 g mol<sup>-1</sup>, while  $f_{PS}$  was maintained constant, the complex adopted a lamellar morphology. The same behavior was noticed with the further increase of the total molar mass of the complex.<sup>32</sup> For the present study we prepared a large number of different PS-*b*-P4VP(PDP)<sub>x</sub> samples to systematically study the phase behavior of the supramolecular system in the region of the phase diagram in which the double gyroid morphology was expected. The systems investigated were divided into three groups according to the ratio between the molar mass of the PS block and the P4VP block in the starting block copolymer (this ratio is designated as *r*). Figure 1 schematically presents the

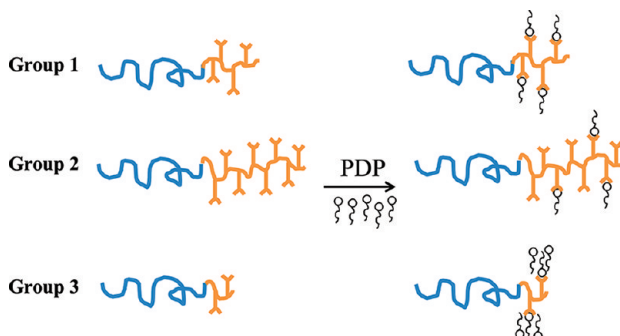


**Figure 1.** Schematic representation of the block copolymer precursors and the corresponding supramolecular complexes from groups 1, 2, and 3. Ratios *r* ( $r = M_n(\text{PS})/M_n(\text{P4VP})$ ) for groups 1, 2, and 3 are  $r \cong 2.45$ ,  $r < 2.45$ , and  $r > 2.45$ , respectively. The double gyroid morphology of the final supramolecular complex is expected for a comb block weight fraction  $f(\text{P4VP}(\text{PDP}))_x$  of ca. 0.62.<sup>32</sup> To achieve this, different relative amounts *x* of PDP have to be added to the block copolymer precursors from groups 1, 2, and 3:  $x \cong 1.0$ ,  $x < 1.0$ , and  $x > 1.0$ , respectively.

block copolymer precursors and the corresponding supramolecular complexes from groups 1, 2, and 3. Ratios *r* for groups 1, 2, and 3 were chosen such that double gyroid morphologies in supramolecular complexes, formed upon the addition of PDP, were expected for  $x = 1.0$ ,  $x < 1.0$ , and  $x > 1.0$ , respectively. In each group, *r* was maintained relatively constant while the molar masses of the PS-*b*-P4VP block copolymers were altered which allowed us to move vertically in the phase diagram.

Additionally, by adjusting the amount of PDP, the weight fractions of the blocks in the supramolecular complexes were changed and we could move along the *x*-axis in the phase diagram. Our aim was to understand which parameter values of the system give rise to the gyroid morphology, how we can tune the size of the gyroid unit cell as well as the porosity of the nanoporous gyroid templates, and what the possible limitations are in terms of the molar masses of the starting block copolymers and the size of the structures obtained.<sup>26,27</sup>

## EXPERIMENTAL SECTION

**Materials.** Diblock copolymers of polystyrene and poly(4-vinylpyridine) were obtained from Polymer Source Inc. The properties of the diblock copolymers studied are listed in Table 1. The polymers

**Table 1. Properties of the Diblock Copolymers PS-*b*-P4VP Used in This Study<sup>a</sup>**

sample code	$M_n(\text{PS})$ , g mol <sup>-1</sup>	$M_n(\text{P4VP})$ , g mol <sup>-1</sup>	<i>r</i>	PDI
Group 1				
S4VP-33.5k-1	24 000	9 500	2.53	1.10
S4VP-45.1k-1	31 900	13 200	2.42	1.08
S4VP-53.5k-1	37 500	16 000	2.34	1.30
S4VP-68.3k-1	48 000	20 300	2.36	1.13
Group 2				
S4VP-21.5k-2	12 000	9 500	1.26	1.09
S4VP-43.5k-2	27 000	16 500	1.64	1.15
S4VP-56.0k-2	35 000	21 000	1.67	1.09
S4VP-65.0k-2	41 000	24 000	1.71	1.09
Group 3				
S4VP-15.0k-3	11 000	4 000	2.75	1.09
S4VP-32.0k-3	25 000	7 000	3.57	1.10
S4VP-67.0k-3	50 000	17 000	2.94	1.15

<sup>a</sup>The division into three groups is made according to the ratio *r* between the molar masses of the PS and the P4VP block. The first number in the sample code denotes the total molar mass of the PS-*b*-P4VP block copolymer, and the second number denotes the group to which it belongs.

were used as received. 3-Pentadecylphenol (PDP) was acquired from Sigma-Aldrich (98 wt % purity) and was recrystallized twice from petroleum ether. Chloroform (p.a., LAB-SCAN) was used as received.

**Preparation of the Polymer Films.** Films of the supramolecular complexes were cast by dissolving the PS-*b*-P4VP diblock copolymer and PDP in chloroform. The concentration of polymer was maintained below 2 wt % to ensure homogeneous complex formation, and the solution was stirred for a couple of hours at room temperature. Afterward, the solution was poured into a glass Petri dish, which was subsequently placed into a saturated chloroform atmosphere. Chloroform was allowed to evaporate slowly during several days at room temperature. Subsequently, the samples were dried in vacuum at 30 °C overnight and annealed several days at 120 °C under N<sub>2</sub> atmosphere with 1 bar overpressure to make sure that the morphology represents the equilibrium structure of the melt state of the PS-*b*-P4VP(PDP) complex. Finally, samples were slowly cooled down to room temperature.

**Characterization.** Transmission electron microscopy was performed on a Philips CM12 transmission electron microscope operating at an accelerating voltage of 120 kV. Images were recorded on a Gatan slow-scan CCD camera. A piece of the film was embedded in an epoxy resin (Epofix, Electron Microscopy Sciences) and cured overnight at 40 °C. The sample was subsequently microtomed to a thickness of about 80 nm using a Leica Ultracut UCT-ultramicrotome and a Diatome diamond knife at room temperature. The microtomed sections were floated on water and subsequently placed on copper grids. To obtain contrast for TEM, the samples were stained with iodine (45 min).

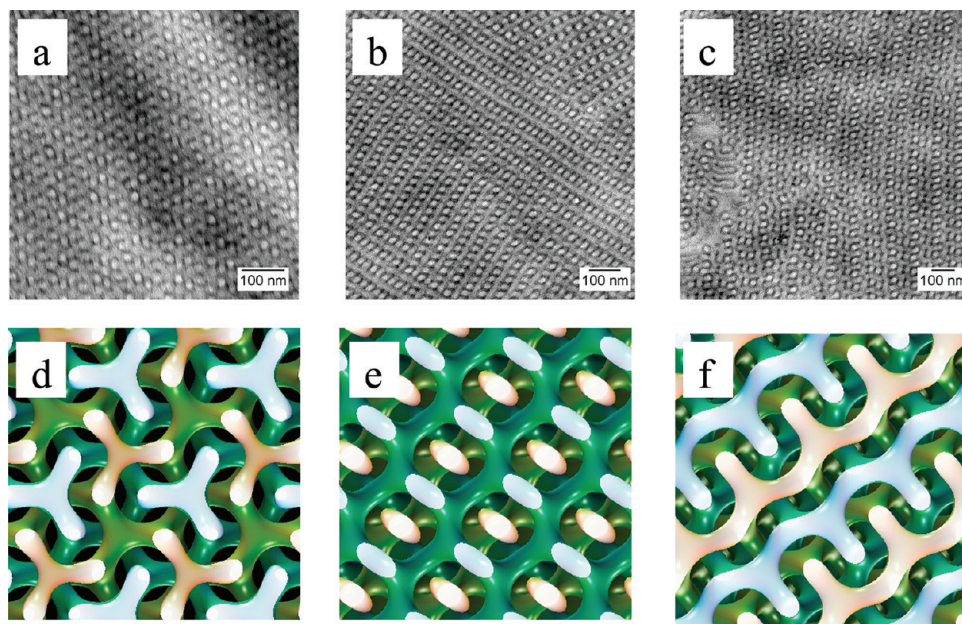


**Figure 2.** Bright-field TEM images of PS-*b*-P4VP(PDP)<sub>1.0</sub>,  $f_{\text{PS}} = 0.38$ ,  $M_{\text{total}} = 83\,300 \text{ g mol}^{-1}$  based on S4VP-45.1k-1; panels a, b, and c represent projections through the (111), (110), and (211) gyroid planes, respectively. TEM simulations of the (111), (110), and (211) planes are given in panels d, e, and f, respectively, as a comparison to experimental data.<sup>35</sup>

Small-angle X-ray scattering (SAXS) was performed on two different setups. The first one was at the Dutch-Belgian Beamlne (DUBBLE) station BM26B of the European Synchrotron Radiation Facility (ESRF) in Grenoble (France). The sample-to-detector distance was ca. 5 m with a wavelength of 1.033 Å. A Dectris-Pilatus 1M detector with a resolution of  $981 \times 1043$  pixels and a pixel size of  $172 \times 172 \mu\text{m}$  has been employed to record the 2D-SAXS scattering patterns. Standard corrections for sample absorption and background subtraction have been performed. The data were normalized with respect to the incident beam intensity in order to correct for primary beam intensity fluctuations. The scattering patterns from rat tail were used for the calibration of the wave vector scale of the scattering curve. The SAXS patterns were acquired at room temperature. The scattering vector  $q$  is defined as  $q = 4\pi/\lambda \sin \theta$  with  $2\theta$  being the scattering angle.<sup>33,34</sup>

The second setup was on the SAXS device in the Nanomicroscopy Center at the Aalto University that consists of a Bruker MICROSTAR microfocus rotating anode X-ray source with Montel Optics (parallel beam, Cu K $\alpha$  radiation  $\lambda = 1.54 \text{ \AA}$ ), where the beam was further collimated using three sets of JJ X-ray 4-blade slits. A sample-to-detector distance of 4.64 m was used. The scattering intensities were measured using a 2D area detector (Bruker HiStar). The samples were measured at room temperature in vacuum.

## RESULTS AND DISCUSSION

The weight fraction  $f$  of the comb block P4VP(PDP) <sub>$x$</sub>  in the supramolecular PS-*b*-P4VP(PDP) <sub>$x$</sub>  complex is related to the mass  $m$  of the different constituents by

$$f(\text{P4VP(PDP)}) = \frac{m(\text{PDP}) + m(\text{P4VP})}{m(\text{PDP}) + m(\text{P4VP}) + m(\text{PS})} \quad (1a)$$

The mass of PDP can be expressed as

$$m(\text{PDP}) = \frac{m(\text{P4VP})}{105 \frac{\text{g}}{\text{mol}}} \times x \times 304 \frac{\text{g}}{\text{mol}} \cong 3x \times m(\text{P4VP}) \quad (1b)$$

Hence

$$f(\text{P4VP(PDP)}) \cong \frac{3x + 1}{3x + 1 + r} \quad (1c)$$

Taking previous experimental results into account,<sup>32</sup> the double gyroid morphology is expected in complexes with a weight fraction of the comblike P4VP(PDP) <sub>$x$</sub>  block of ca. 0.62.

**Morphological Characterization of the PS-*b*-P4VP(PDP) <sub>$x$</sub>  Samples from Group 1.** When a stoichiometric ratio between PDP molecules and P4VP monomer units ( $x = 1.0$ ) is aimed for, block copolymers with a ratio  $r$  between molar masses of PS and P4VP block of ca. 2.45 should be used as a precursors for the preparation of supramolecular complexes with potentially double gyroid morphology. The polymers of group 1 (Table 1) have been selected accordingly.

As reported before, our SAXS and TEM investigations confirm that the supramolecular complex PS-*b*-P4VP(PDP)<sub>1.0</sub> ( $f_{\text{PS}} = 0.38$ ,  $M_{\text{total}} = 83\,300 \text{ g mol}^{-1}$ )<sup>32</sup> prepared from S4VP-45.1k-1 ( $M_n(\text{PS}) = 31\,900 \text{ g mol}^{-1}$ ,  $M_n(\text{P4VP}) = 13\,200 \text{ g mol}^{-1}$ ) forms a double gyroid morphology. Bright-field TEM images representing projections through the (111), (110), and (211) planes of the gyroid unit cell are presented in Figures 2a, 2b, and 2c, respectively. The PS domains appear bright while the P4VP(PDP)<sub>1.0</sub> domains appear dark due to the iodine staining. Computer-simulated projections (Figures 2d, 2e, and 2f) of cross sections, cut parallel to (111), (110), and (211) gyroid planes, respectively, are obtained by TEMsim<sup>35</sup> and show a good agreement with the experimental data. The typical gyroid patterns, the “wagon wheel” (Figures 2a and 2d) and the “double wave” pattern (Figures 2c and 2f), confirm the morphological assignment. SAXS analysis (Figure 3) of the sample supports the TEM data. The first two reflections are positioned in the  $q$  ratio  $\sqrt{6}:\sqrt{8}$ , and they are attributed to the (211) and (220) spacings of the double gyroid morphology. The intensity ratio 10:1 between the first two peaks is a good indication of the bicontinuous  $Ia\bar{3}d$  morphology (as discussed in the literature).<sup>3</sup> The first intensity maximum is centered at

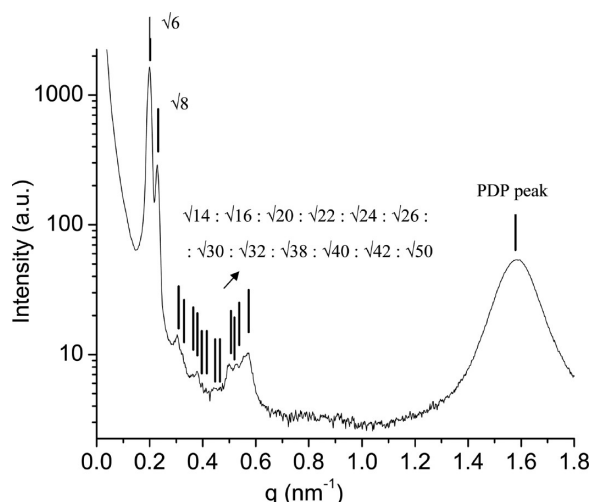


**Figure 3.** SAXS pattern of PS-*b*-P4VP(PDP)<sub>1.0</sub>,  $f_{\text{PS}} = 0.38$ ,  $M_{\text{total}} = 83\,300 \text{ g mol}^{-1}$  based on S4VP-45.1k-1. Lines indicate the expected reflections for the gyroid phase (cubic  $Ia\bar{3}d$  symmetry), and they are positioned in the ratio  $\sqrt{6}:\sqrt{8}:\sqrt{14}:\sqrt{16}:\sqrt{20}:\sqrt{22}:\sqrt{24}:\sqrt{26}:\sqrt{30}:\sqrt{32}:\sqrt{38}:\sqrt{40}:\sqrt{42}:\sqrt{50}$ . The reflection at  $q = 1.58 \text{ nm}^{-1}$  corresponds to the lamellar self-assembly within the P4VP(PDP)<sub>1.0</sub> domains.

$q = 0.199 \text{ nm}^{-1}$  corresponding to the  $d_{211}$  spacing equal to 31.6 nm and the lattice parameter  $a$  of 77.3 nm ( $a = \sqrt{6}d_{211}$ ). Higher order gyroid peaks, although with relatively low intensity, are readily visible in the SAXS pattern (Figure 3). A peak centered at  $q = 1.58 \text{ nm}^{-1}$  corresponds to lamellar structures with the lamellar period of 4 nm, formed in the comblike P4VP(PDP)<sub>1.0</sub> complex

due to the microphase separation between the nonpolar PDP alkyl tails and the polar backbone.<sup>36</sup>

The block copolymer S4VP-33.5k-1 ( $M_n(\text{PS}) = 24\,000 \text{ g mol}^{-1}$ ,  $M_n(\text{P4VP}) = 9500 \text{ g mol}^{-1}$ ) with shorter blocks but similar ratio between the molar masses of the PS and P4VP blocks is used to prepare a set of supramolecular samples by systematically changing the amount of PDP from 0.5 to 1.7, thus reducing  $f_{\text{PS}}$  from 0.51 to 0.30. As a function of  $x$ , the morphology of the complex changes along the pathway LAM ( $0.5 \leq x \leq 0.8$ )  $\rightarrow$  GYR ( $0.9 \leq x \leq 1.0$ )  $\rightarrow$  CYL ( $1.1 \leq x \leq 1.7$ ). Figure 4 shows representative TEM images. Well-aligned lamellae of the sample with  $x = 0.7$  are shown in Figure 4a. Figure 4b presents the projection through the (110) plane of the gyroid sample ( $x = 1.0$ ), and hexagonally ordered cylinders of the sample with  $x = 1.3$  are depicted in Figure 4c. The bicontinuous  $Ia\bar{3}d$  morphology is found in the composition range  $\Delta f_{\text{PS}} \geq 0.02$  ( $f_{\text{PS}} = 0.41$  for  $x = 0.9$  and  $f_{\text{PS}} = 0.39$  for  $x = 1.0$ ). SAXS patterns of two gyroid samples from this range are shown in Figure 5. The  $q$  ratios of  $\sqrt{6}:\sqrt{8}$  and intensity ratios of nearly 10:1 between the first two reflections represent an unambiguous signature of the double gyroid morphology. The first-order reflections are equally positioned for both samples at  $q = 0.216 \text{ nm}^{-1}$ , indicating the size of the unit cells to be 71.2 nm. This implies that the small variation of the PDP amount does not affect the size of the unit cell which can be exploited for the preparation of porous templates with the same interdomain spacing but somewhat different porosity. As calculated, the porosity of the templates prepared from these particular complexes can be varied from 42.5% to 45.1%. However, the size of the gyroid unit cell is influenced by the total molar mass of the starting copolymer, which allows us to

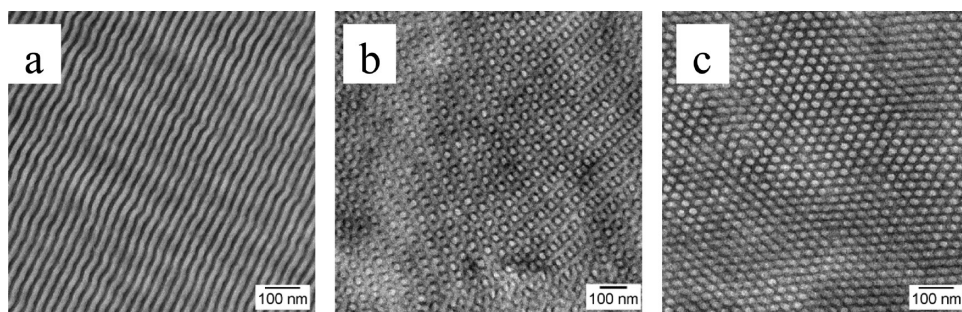


**Figure 4.** Bright-field TEM images of PS-*b*-P4VP(PDP)<sub>x</sub> complexes prepared from the diblock copolymer S4VP-33.5k-1 with  $x$  values of (a) 0.7, (b) 1.0, and (c) 1.3.

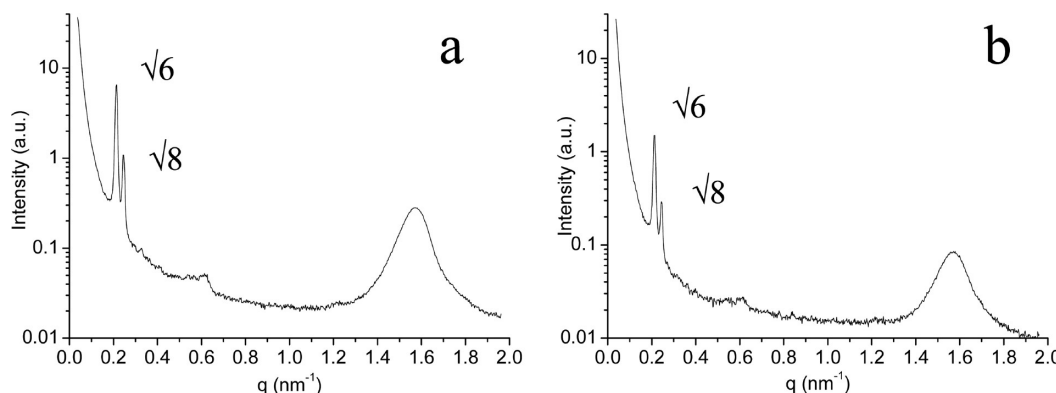


**Figure 5.** SAXS patterns of PS-*b*-P4VP(PDP)<sub>x</sub> complexes with a double gyroid morphology. The samples are prepared from the diblock copolymer S4VP-33.5k-1 and have  $x$  = (a) 0.9 and (b) 1.0.

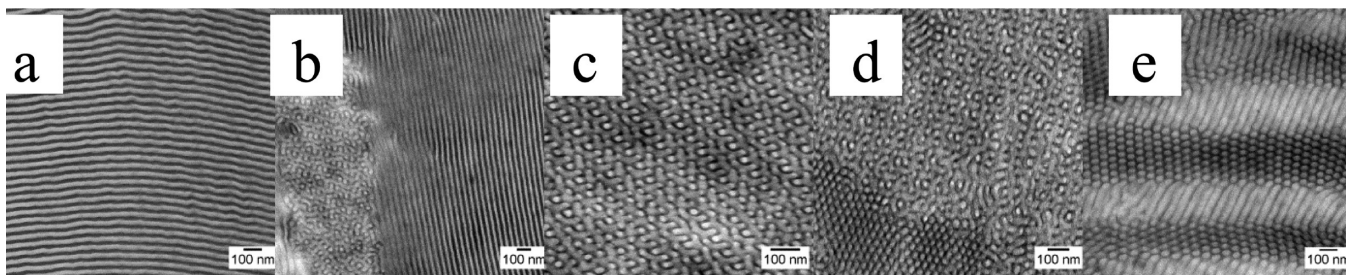


**Figure 6.** Bright-field TEM images of PS-*b*-P4VP(PDP)<sub>x</sub> complexes prepared from the diblock copolymer S4VP-53.5k-1 with  $x$  values of (a) 0.6, (b) 0.7, (c) 0.8, (d) 0.9, and (e) 1.0.

adjust the lattice parameter by varying the molar mass of the block copolymer precursor.

To further investigate the phase behavior of the supramolecular complex PS-*b*-P4VP(PDP)<sub>x</sub>, another set of samples is prepared starting from the diblock copolymer with longer blocks S4VP-53.5k-1 ( $M_n(\text{PS}) = 37\,500 \text{ g mol}^{-1}$ ,  $M_n(\text{P4VP}) = 16\,000 \text{ g mol}^{-1}$ ). The PDP content is varied from  $x = 0.5$  to  $x = 1.5$ , which implies a change in the weight fraction of the PS block from 0.49 to 0.30. The morphology of the complexes changes as follows: LAM ( $0.5 \leq x \leq 0.6$ )  $\rightarrow$  LAM + GYR ( $x = 0.7$ )  $\rightarrow$  GYR ( $x = 0.8$ )  $\rightarrow$  GYR + CYL ( $x = 0.9$ )  $\rightarrow$  CYL ( $1.0 \leq x \leq 1.5$ ). Bright-field TEM images of several representative samples are given in Figure 6. Equally thick alternating PS and P4VP(PDP) lamellae of the sample with  $x = 0.6$  are shown in Figure 6a, the gyroid "double wave" pattern of the sample with  $x = 0.8$  is depicted in Figure 6c, and hexagonally packed cylinders of the sample with  $x = 1.0$  are represented in Figure 6e. Additionally, biphasic morphologies appear as transitional phases between the lamellar and the gyroid phase (Figure 6b, sample with  $x = 0.7$ ) as well as between the gyroid and the cylindrical phase (Figure 6d, sample with  $x = 0.9$ ). Biphasic morphologies do not really come as a surprise since theoretical studies on related supramolecular diblock copolymers show their presence in the phase diagram due to the supramolecular nature of the system.<sup>37,38</sup> Grain boundaries between the two coexisting phases can be easily observed in the TEM images. The double gyroid morphology is confirmed in one sample ( $x = 0.8$ ), and if a slight horizontal move to any side in the phase diagram is made (to  $x = 0.7$  or  $x = 0.9$ ), the complexes enter the biphasic region. If this is compared with the previously discussed results (Figures 4 and 5), we notice a contraction of the gyroid region with an increase of the molar mass of the block copolymer precursor, as in the case of simple diblock copolymers.<sup>18</sup> The phase behavior of the complexes is further examined by SAXS. The first-order reflection of the lamellar sample (Figure 7) appears at  $q^* = 0.148 \text{ nm}^{-1}$  (hence, lamellar period is 42.4 nm), and another reflection is found at the position  $3q^*$ . Even-order reflections ( $2q^*$ ,  $4q^*$ ,  $6q^*$ , etc.) are absent due to the symmetry of the alternating lamellae having equal thickness.<sup>39</sup> In the SAXS pattern of the gyroid sample, the peaks are found at the following positions:  $\sqrt{6}q^*$ ,  $\sqrt{8}q^*$ ,  $\sqrt{14}q^*$ ,  $\sqrt{22}q^*$ , and  $\sqrt{50}q^*$  as indicated with arrows. The first reflection of the gyroid sample coincides with the first reflection of the lamellar sample, implying the size of the gyroid unit cell to be 104 nm. The SAXS pattern of the sample with a coexisting lamellar and gyroid phase is also shown in Figure 7, and it is expected to represent a superposition of the former two patterns. The  $\sqrt{6}:\sqrt{8}$   $q$  ratio between the first two reflections and higher order peaks indicated with arrows confirm the

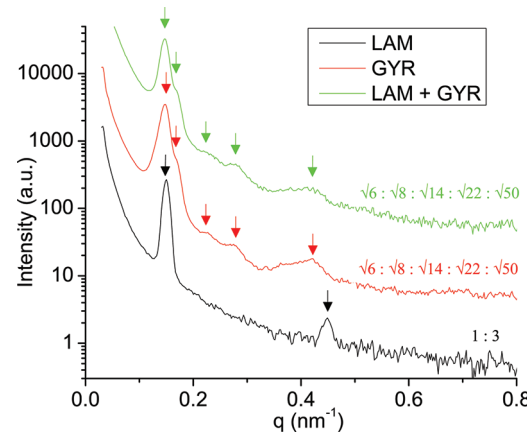


**Figure 7.** SAXS patterns of PS-*b*-P4VP(PDP)<sub>x</sub> complexes prepared from the diblock copolymer S4VP-53.5k-1 with  $x = 0.6$  (black line),  $x = 0.7$  (green line), and  $x = 0.8$  (red line).

existence of the double gyroid regions in the sample. It is rather difficult to confirm the presence of the lamellar phase from SAXS results, since the  $3q^*$  lamellar peak would be the only signal to contribute to the SAXS pattern, and it is positioned closely to the gyroid  $\sqrt{50}q^*$  peak. The first peak in the SAXS pattern of the cylindrical sample (Figure 8) is centered at

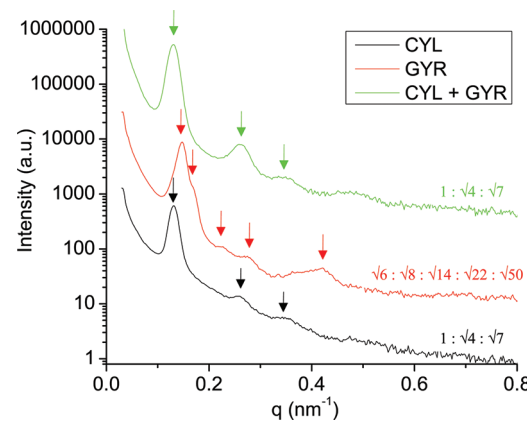


**Figure 8.** SAXS patterns of PS-*b*-P4VP(PDP)<sub>x</sub> complexes prepared from the diblock copolymer S4VP-53.5k-1 with  $x = 0.8$  (red line),  $x = 0.9$  (green line), and  $x = 1.0$  (black line).

$q^* = 0.131 \text{ nm}^{-1}$  (hence, the calculated distance between the cylinders is 55.4 nm), and higher order peaks positioned at  $\sqrt{4}q^*$  and  $\sqrt{7}q^*$  confirm the morphological assignment. An identical SAXS pattern with well-defined higher order cylindrical peaks is found in the sample with a coexisting

cylindrical and gyroid phase. The absence of gyroid peaks in the biphasic sample could imply that the cylinders represent the majority phase or that the gyroid phase has a low degree of ordering. To better resolve the first two reflections, the gyroid sample was measured for longer time (90 h), and the result is provided in the Supporting Information (Figure 1). Two signals positioned in the  $q$  ratio  $\sqrt{6}:\sqrt{8}$  ( $q_1 = 0.148 \text{ nm}^{-1}$  and  $q_2 = 0.171 \text{ nm}^{-1}$ ) can be clearly observed.

To examine the phase behavior of complexes with even higher molar mass and thus stronger segregation, a series of samples with  $x$  ranging from 1.0 to 1.7 is prepared from the block copolymer precursor S4VP-68.3k-1 ( $M_n(\text{PS}) = 48\,000 \text{ g mol}^{-1}$ ,  $M_n(\text{P4VP}) = 20\,300 \text{ g mol}^{-1}$ ). Here a direct transition from the lamellar to the cylindrical phase is found: LAM ( $1.0 \leq x \leq 1.1$ )  $\rightarrow$  CYL ( $1.2 \leq x \leq 1.7$ ), and the double gyroid morphology is not observed anymore. Representative TEM images are given in Figure 9. This suggests that the double

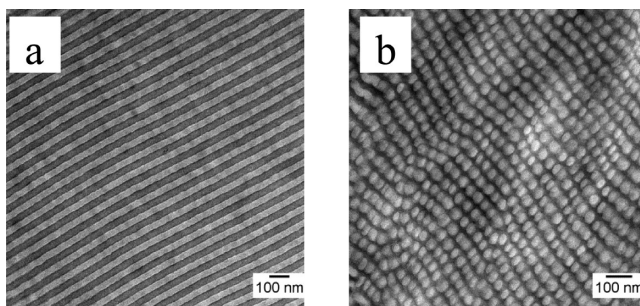


**Figure 9.** Bright-field TEM images of  $\text{PS-}b\text{-P4VP(PDP)}_x$  complexes prepared from the diblock copolymer S4VP-53.5k-1 with values of  $x$  = (a) 1.0 and (b) 1.5.

gyroid phase does not exist in supramolecular complexes  $\text{PS-}b\text{-P4VP(PDP)}_x$  based on block copolymer precursors of group 1 if the molar mass of the starting block copolymer exceeds a critical value.

The morphological characterization of  $\text{PS-}b\text{-P4VP(PDP)}_x$  complexes from group 1 is summarized in Figure 10 and Table 2.

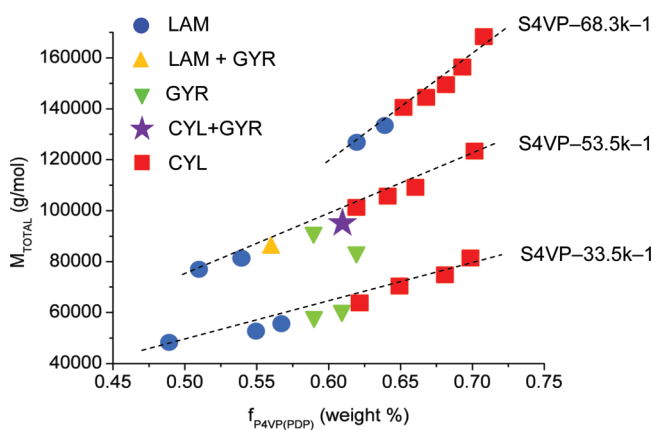


**Figure 10.** Phase diagram of supramolecular complexes  $\text{PS-}b\text{-P4VP(PDP)}_x$  from group 1. The total molar mass of the complex is given on the  $y$ -axis while the weight fraction of the comb block is given on the  $x$ -axis. Samples connected with dashed lines are prepared from the same block copolymer precursor with code as given.

#### Morphological Characterization of the $\text{PS-}b\text{-P4VP(PDP)}_x$ Samples from Group 2.

This group of systems is of

**Table 2. Morphological Characterization of Supramolecular Complexes  $\text{PS-}b\text{-P4VP(PDP)}_x$  from Group 1**

block copolymer code	$x$	$f_{\text{PS}}$	morphology
S4VP-45.1k-1	1.0	0.38	GYR
S4VP-33.5k-1	0.5	0.51	LAM
S4VP-33.5k-1	0.7	0.45	LAM
S4VP-33.5k-1	0.8	0.43	LAM
S4VP-33.5k-1	0.9	0.41	GYR
S4VP-33.5k-1	1.0	0.39	GYR
S4VP-33.5k-1	1.1	0.38	CYL
S4VP-33.5k-1	1.3	0.35	CYL
S4VP-33.5k-1	1.5	0.32	CYL
S4VP-33.5k-1	1.7	0.30	CYL
S4VP-53.5k-1	0.5	0.49	LAM
S4VP-53.5k-1	0.6	0.46	LAM
S4VP-53.5k-1	0.7	0.44	LAM + GYR
S4VP-53.5k-1	0.8	0.41	GYR
S4VP-53.5k-1	0.9	0.39	GYR + CYL
S4VP-53.5k-1	1.0	0.38	CYL
S4VP-53.5k-1	1.1	0.36	CYL
S4VP-53.5k-1	1.2	0.34	CYL
S4VP-53.5k-1	1.5	0.30	CYL
S4VP-68.3k-1	1.0	0.38	LAM
S4VP-68.3k-1	1.1	0.36	LAM
S4VP-68.3k-1	1.2	0.35	CYL
S4VP-68.3k-1	1.3	0.33	CYL
S4VP-68.3k-1	1.4	0.32	CYL
S4VP-68.3k-1	1.5	0.31	CYL
S4VP-68.3k-1	1.7	0.29	CYL

special interest since now the gyroid morphology is expected for  $x < 1$ . As has been demonstrated before, PDP molecules can be easily removed from the gyroid supramolecular complex  $\text{PS-}b\text{-P4VP(PDP)}_x$  by selective dissolution. We are interested in applications where the porous nanotemplate is backfilled with metal, and subsequently, the polymer support is removed via pyrolysis to create well-ordered metal nanofoams with the inverse gyroid morphology. Since the porosity is inversely proportional to the amount of PDP in the starting supramolecular complex, values of  $x$  smaller than 1 are of specific interest.<sup>31</sup> A higher surface area, thus higher porosity of the metallic foam, is desirable for many applications, such as catalysts or actuators. As a guideline for the appearance of the gyroid phase we again prepare samples around  $f_{\text{P4VP(PDP)}} \approx 0.62$ .

The total number of monomer units in the block copolymer precursors of group 2 varies from ca. 215 to 650, and as will be shown, the double gyroid morphology is indeed found in several samples. The TEM image and the SAXS pattern of a representative sample  $\text{PS-}b\text{-P4VP(PDP)}_{0.75}$  prepared from the diblock copolymer S4VP-65.0k-2 are given in Figure 11. The gyroid reflections  $\sqrt{6}q^*$ ,  $\sqrt{8}q^*$ ,  $\sqrt{30}q^*$ ,  $\sqrt{38}q^*$ , and  $\sqrt{50}q^*$  are resolved in the SAXS pattern (Figure 9b). The lattice parameter  $a = 124 \text{ nm}$ , as calculated from the position of the first-order reflection at  $q = 0.124 \text{ nm}^{-1}$ . The TEM image (Figure 11a) represents the typical “wagon wheel” gyroid pattern.

In supramolecular complexes prepared from the diblock copolymer with the shortest blocks S4VP-21.5k-2 ( $M_n(\text{PS}) = 12\,000 \text{ g mol}^{-1}$ ,  $M_n(\text{P4VP}) = 9500 \text{ g mol}^{-1}$ ), the double gyroid phase is found for  $x = 0.40$ , and when  $x$  is changed by  $\pm 0.05$ , the complex adopts a lamellar and cylindrical morphology.

For the  $\text{PS-}b\text{-P4VP}$  precursors with higher molar mass biphasic morphologies are mostly found. TEM images of samples

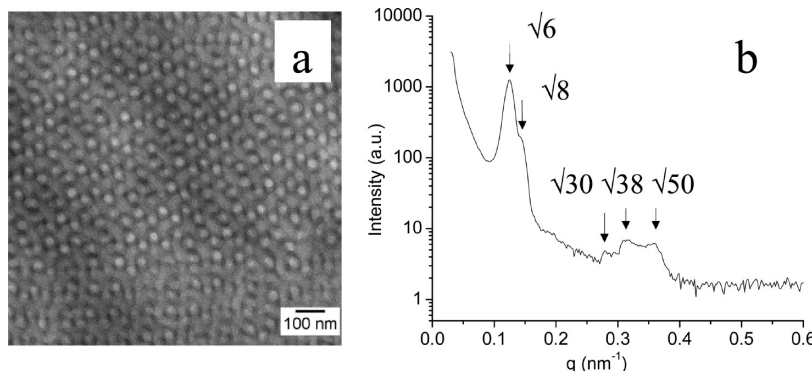


**Figure 11.** PS-*b*-P4VP(PDP)<sub>0.75</sub> complex prepared from the diblock copolymer S4VP-65.0k-2: (a) bright-field TEM image representing the projection through the gyroid (111) plane; (b) SAXS pattern of the gyroid sample.

with two coexisting phases are shown in Figure 12. Figure 12a shows a combination of lamellae and gyroids for a sample based

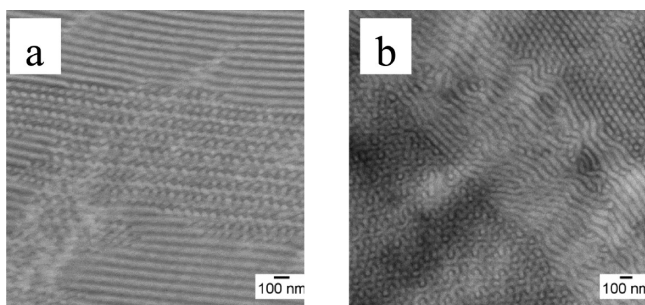


**Figure 12.** Bright-field TEM images of PS-*b*-P4VP(PDP)<sub>x</sub> complexes: (a) S4VP-56.0k-2 precursor,  $x = 0.53$ ; (b) S4VP-65.0k-2 precursor,  $x = 0.7$ .

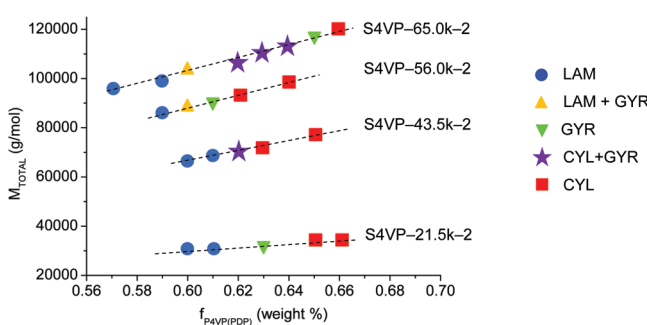


**Figure 13.** Phase diagram of supramolecular complexes PS-*b*-P4VP(PDP)<sub>x</sub> from group 2. The total molar mass of the complex is given at the *y*-axis while the weight fraction of a comb block is given at the *x*-axis. Samples connected with a dashed line are prepared from the same block copolymer precursor with the code as given.

on the S4VP-56.0k-2 precursor, whereas well-ordered grains of the gyroid and the cylindrical phase, separated by a transitional phase of poorly ordered cylinders, is depicted in Figure 12b for a sample based on the S4VP-65.0k-2 precursor. Much to our surprise, we observed the sequence GYR + CYL → GYR → CYL rather than the anticipated GYR → GYR + CYL → CYL sequence for the samples prepared from the highest molar mass S4VP-65.0k-2. As an additional surprise, the GYR + CYL region becomes broader with an increase of the molar mass of the block copolymer precursor. This demonstrates the complex nature of the system as compared to simple diblock copolymers. Not only

do we have a comblike molecular architecture of the supramolecular block, but in addition the effective interaction between PS and P4VP(PDP)<sub>x</sub>, and therefore the degree of segregation, depends on the relative amount of PDP, i.e.  $x$ .

The morphological characterization of PS-*b*-P4VP(PDP)<sub>x</sub> complexes from group 2 is summarized in Figure 13 and Table 3.

**Table 3. Morphological Characterization of Supramolecular Complexes PS-*b*-P4VP(PDP)<sub>x</sub> from Group 2**

block copolymer code	$x$	$f_{PS}$	morphology
S4VP-21.5k-2	0.3	0.40	LAM
S4VP-21.5k-2	0.35	0.39	LAM
S4VP-21.5k-2	0.4	0.37	GYR
S4VP-21.5k-2	0.45	0.35	CYL
S4VP-21.5k-2	0.5	0.34	CYL
S4VP-21.5k-2	1.0	0.24	CYL
S4VP-43.5k-2	0.5	0.40	LAM
S4VP-43.5k-2	0.53	0.39	LAM
S4VP-43.5k-2	0.57	0.38	GYR + CYL
S4VP-43.5k-2	0.6	0.37	CYL
S4VP-43.5k-2	0.7	0.35	CYL
S4VP-56.0k-2	0.5	0.41	LAM
S4VP-56.0k-2	0.53	0.40	LAM + GYR
S4VP-56.0k-2	0.57	0.39	GYR
S4VP-56.0k-2	0.6	0.38	CYL
S4VP-56.0k-2	0.7	0.36	CYL
S4VP-65.0k-2	0.45	0.43	LAM
S4VP-65.0k-2	0.5	0.41	LAM
S4VP-65.0k-2	0.55	0.40	LAM + GYR
S4VP-65.0k-2	0.6	0.38	GYR + CYL
S4VP-65.0k-2	0.65	0.37	GYR + CYL
S4VP-65.0k-2	0.7	0.36	GYR + CYL
S4VP-65.0k-2	0.75	0.35	GYR
S4VP-65.0k-2	0.8	0.34	CYL

**Morphological Characterization of the PS-*b*-P4VP(PDP)<sub>x</sub> Samples from Group 3.** Finally, we discuss the morphology of PS-*b*-P4VP(PDP)<sub>x</sub> complexes where a gyroid morphology is anticipated to occur for an excess of PDP molecules with respect to the number of pyridine groups. PS-*b*-P4VP polymers with ca. 150, 320, and 670 monomer units in total and  $r > 2.45$  (Table 1, group 3) are used for this purpose.

Complexes produced from the polymer precursor S4VP-15.0k-3 ( $M_n(\text{PS}) = 11\,000 \text{ g mol}^{-1}$ ,  $M_n(\text{P4VP}) = 4000 \text{ g mol}^{-1}$ ) with  $N = 150$  and  $1.1 \leq x \leq 1.5$  ( $0.40 \geq f_{PS} \geq 0.34$ ) have a disordered microphase separated morphology as shown by

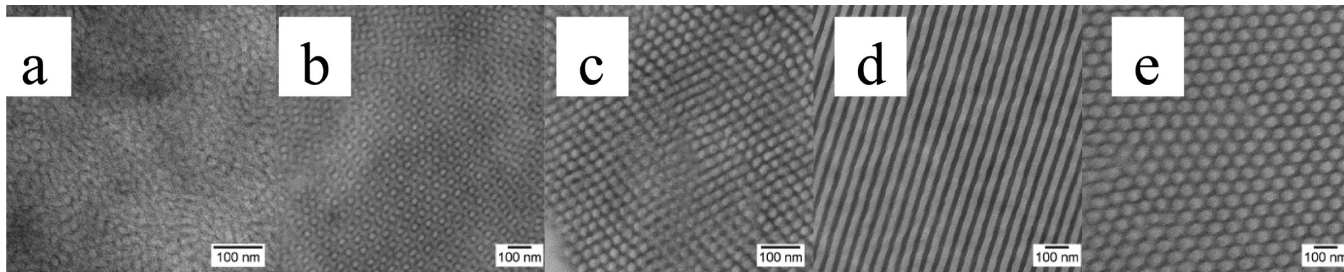


**Figure 14.** Bright-field TEM images of PS-*b*-P4VP(PDP)<sub>x</sub> complexes: (a) S4VP-15.0k-3 precursor,  $x = 1.1$ ; (b, c) S4VP-32.0k-3 precursor,  $x = 1.6$ ; (d) S4VP-67.0k-3 precursor,  $x = 1.1$ ; (e) S4VP-67.0k-3 precursor,  $x = 1.5$ .

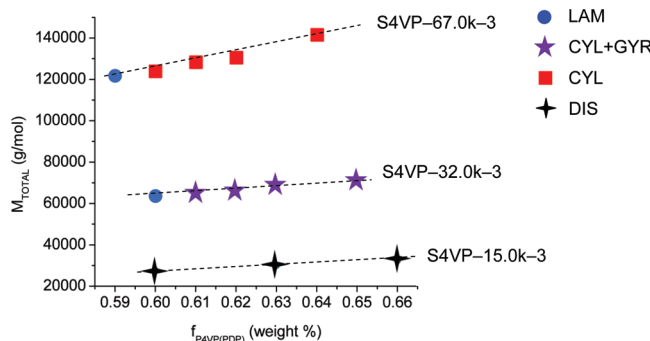


**Figure 15.** Phase diagram of supramolecular complexes PS-*b*-P4VP(PDP)<sub>x</sub> from group 3. The total molar mass of the complex is given at the *y*-axis while the weight fraction of a comb block is given at the *x*-axis. Samples connected with a dashed line are prepared from the same block copolymer precursor with code as given.

**Table 4. Morphological Characterization of Supramolecular Complexes PS-*b*-P4VP(PDP)<sub>x</sub> from Group 3**

block copolymer code	$x$	$f_{\text{PS}}$	morphology
S4VP-15.0k-3	1.1	0.40	DIS
S4VP-15.0k-3	1.3	0.37	DIS
S4VP-15.0k-3	1.5	0.34	DIS
S4VP-32.0k-3	1.5	0.40	LAM
S4VP-32.0k-3	1.6	0.39	GYR + CYL
S4VP-32.0k-3	1.7	0.38	GYR + CYL
S4VP-32.0k-3	1.8	0.37	GYR + CYL
S4VP-32.0k-3	1.9	0.35	GYR + CYL
S4VP-67.0k-3	1.1	0.41	LAM
S4VP-67.0k-3	1.17	0.40	CYL
S4VP-67.0k-3	1.24	0.39	CYL
S4VP-67.0k-3	1.3	0.38	CYL
S4VP-67.0k-3	1.5	0.36	CYL

TEM (Figure 14a). The value of the interaction parameter between PS and P4VP is on the order of  $\chi_{\text{S},\text{4VP}} \cong 0.35$ .<sup>40,41</sup> Therefore, for the polymer precursor  $\chi N \cong 50$ , well within the ordered range. The disordered microphase-separated structures of the complexes confirm once again that the addition of PDP to PS-*b*-P4VP reduces the effective interaction parameter between the two phases, PS and P4VP(PDP), respectively.<sup>31</sup>

Samples obtained from the precursor S4VP-32.0k-3 ( $M_n(\text{PS}) = 25\,000 \text{ g mol}^{-1}$ ,  $M_n(\text{P4VP}) = 7\,000 \text{ g mol}^{-1}$ ) with  $x$  ranging from 1.5 to 1.9 ( $f_{\text{PS}}$  varies from 0.40 to 0.35) exhibit a lamellar morphology LAM for  $x = 1.5$  and a rather broad biphasic GYR + CYL region for  $1.6 \leq x \leq 1.9$ . Figures 14b and 14c present a gyroid grain (projection through the (110) plane) and a cylindrical grain as found in a representative biphasic sample ( $x = 1.6$ ).

If the starting block copolymer has a sufficiently high molar mass (S4VP-67.0k-3,  $M_n(\text{PS}) = 50\,000 \text{ g mol}^{-1}$ ,  $M_n(\text{P4VP}) = 17\,000 \text{ g mol}^{-1}$ ) a direct transition from the lamellar to the cylindrical phase is found: LAM ( $x = 1.1$ ) → CYL ( $1.17 \leq x \leq 1.5$ ). Representative TEM images are provided in Figures 14d and 14e.

The morphological characterization of PS-*b*-P4VP(PDP)<sub>x</sub> complexes from group 3 is summarized in Figure 15 and Table 4.

## CONCLUSION

A comprehensive study of the phase behavior of supramolecular complexes PS-*b*-P4VP(PDP)<sub>x</sub> from three different groups where the double gyroid morphology is anticipated to occur at  $x < 1.0$ ,  $x = 1.0$  and  $x > 1.0$ , respectively, has been conducted. A number of samples exhibiting the double gyroid network morphology were found. The morphological characterization of the complexes from group 1 (gyroid morphology expected for  $x \cong 1.0$ ) indicated a contraction of the width of the gyroid region with an increase in molar mass of the polymer precursor PS-*b*-P4VP, followed by the absence of the cubic  $Ia\bar{3}d$  symmetry above a critical value. This was also found for the samples from group 3 ( $x > 1.0$ ). Samples from group 2 behaved differently, in the sense that for the highest molar mass employed a large biphasic window was found with one of the phases being the gyroid phase. Of course, it cannot be excluded that also for this group the gyroid morphology will cease to exist for even higher molar masses.

The size of the gyroid unit cell was tuned by varying the molar mass of the starting block copolymer from  $a = 71.2 \text{ nm}$  to  $a = 124 \text{ nm}$ . The porosities of the nanoporous templates obtained from gyroid supramolecular complexes PS-*b*-P4VP-(PDP)<sub>x</sub> by dissolving PDP can be tuned as well since the cubic  $Ia\bar{3}d$  symmetry appeared in samples from all three groups, i.e.,  $x < 1.0$ ,  $x = 1.0$ , and  $x > 1.0$ . The results of this study show how to prepare double gyroid templates with tailored feature sizes and porosities.

## ASSOCIATED CONTENT

### S Supporting Information

Figure 1. This material is available free of charge via the Internet at <http://pubs.acs.org>.

## AUTHOR INFORMATION

### Corresponding Author

\*E-mail: k.u.loos@rug.nl (K.L.); g.ten.brinke@rug.nl (G.t.B.).

### Notes

The authors declare no competing financial interest.

## ACKNOWLEDGMENTS

We acknowledge Marc Stuart for his help with TEM.

## REFERENCES

- (1) Szwarc, M. 'Living' Polymers. *Nature* **1956**, *178*, 1168–1169.
- (2) Bates, F. S.; Fredrickson, G. H. Block Copolymer Thermodynamics: Theory and Experiment. *Annu. Rev. Phys. Chem.* **1990**, *41*, 525–527.
- (3) Hajduk, D. A.; Harper, P. E.; Gruner, S. M.; Honeker, C. C.; Kim, G.; Thomas, E. L.; Fetters, L. J. The Gyroid: A New Equilibrium Morphology in Weakly Segregated Diblock Copolymers. *Macromolecules* **1994**, *27*, 4063–4075.
- (4) Schulz, M. F.; Bates, F. S.; Almdal, K.; Mortensen, K. Epitaxial Relationship for Hexagonal-to-Cubic Phase Transition in a Block Copolymer Mixture. *Phys. Rev. Lett.* **1994**, *73*, 86–89.
- (5) Hamley, I. W. *The Physics of Block Copolymers*; Oxford University Press: Oxford, 1998.
- (6) Meuler, A. J.; Hillmyer, M. A.; Bates, F. S. Ordered Network Mesosstructures in Block Polymer Materials. *Macromolecules* **2009**, *42*, 7221–7250.
- (7) Bates, F. S.; Fredrickson, G. H. Block Copolymers—Designer Soft Materials. *Phys. Today* **1999**, *52*, 32–38.
- (8) Epps, T. H. III; Cochran, E. W.; Bailey, T. S.; Waletzko, R. S.; Hardy, C. M.; Bates, F. S. Ordered Network Phases in Linear Poly(isoprene-b-styrene-b-ethylene oxide) Triblock Copolymers. *Macromolecules* **2004**, *37*, 8325–8341.
- (9) Abetz, V.; Simon, P. F. W. Phase Behavior and Morphologies of Block Copolymers. *Adv. Polym. Sci.* **2005**, *189*, 125–212.
- (10) Tyler, C. A.; Qin, J.; Bates, F. S.; Morse, D. C. SCFT Study of Nonfrustrated ABC Triblock Copolymer Melts. *Macromolecules* **2007**, *40*, 4654–4668.
- (11) Matsushita, Y. Creation of Hierarchically Ordered Nanophase Structures in Block Polymers Having Various Competing Interactions. *Macromolecules* **2007**, *40*, 771–776.
- (12) Gobius du Sart, G.; Vukovic, I.; Alberda van Ekenstein, G. O. R.; Polushkin, E.; Loos, K.; ten Brinke, G. Self-Assembly of Supramolecular Triblock Copolymer Complexes. *Macromolecules* **2010**, *43* (6), 2970–2980.
- (13) Faber, M.; Voet, V. S. D.; ten Brinke, G.; Loos, K. Preparation and Self-Assembly of Two-Length-Scale A-b-(B-b-A)<sub>n</sub>-b-B Multiblock Copolymers. *Soft Matter* **2012**, *8*, 4479.
- (14) Crossland, E. J. W.; Kamperman, M.; Nedelcu, M.; Ducati, C.; Wiesner, U.; Smilgies, D. M.; Toombes, G. E. S.; Hillmyer, M. A.; Ludwigs, S.; Steiner, U.; Snaith, H. J. A Bicontinuous Double Gyroid Hybrid Solar Cell. *Nano Lett.* **2009**, *9*, 2807–2812.
- (15) Hsueh, H. Y.; Chen, H. Y.; She, M. S.; Chen, C. K.; Ho, R. M.; Gwo, S.; Hasegawa, H.; Thomas, E. L. Inorganic Gyroid with Exceptionally Low Refractive Index from Block Copolymer Templating. *Nano Lett.* **2010**, *10*, 4994–5000.
- (16) Urbas, A. M.; Maldovan, M.; DeRege, P.; Thomas, E. L. Bicontinuous Cubic Block Copolymer Photonic Crystals. *Adv. Mater.* **2002**, *14*, 1850–1853.
- (17) Vignolini, S.; Yu, N. A.; Cunha, P. S.; Guldin, S.; Rushkin, I.; Stefik, M.; Hur, K.; Wiesner, U.; Baumberg, J. J.; Steiner, U. A 3D Optical Metamaterial Made by Self-Assembly. *Adv. Mater.* **2011**, DOI: 10.1002/adma.201103610.
- (18) Cochran, E. W.; Garcia-Cervera, C. J.; Fredrickson, G. H. Stability of the Gyroid Phase in Diblock Copolymers at Strong Segregation. *Macromolecules* **2006**, *39*, 2449–2451.
- (19) Matsen, M. W. Phase behavior of block copolymer/homopolymer blends. *Macromolecules* **1995**, *28* (17), 5765–5773.
- (20) Hayashida, K.; Takano, A.; Arai, S.; Shinohara, Y.; Amemiya, Y.; Matsushita, Y. Systematic Transitions of Tiling Patterns Formed by ABC Star-Shaped Terpolymers. *Macromolecules* **2006**, *39* (26), 9402–9408.
- (21) Lo, C. T.; Lee, B.; Pol, V. G.; Dietz Rago, N. L.; Seifert, S.; Winans, R. E.; Thiagarajan, P. Effect of Molecular Properties of Block Copolymers and Nanoparticles on the Morphology of Self-Assembled Bulk Nanocomposites. *Macromolecules* **2007**, *40* (23), 8302–8310.
- (22) Ajdari, A.; Leibler, L. Bending moduli and stability of copolymer bilayers. *Macromolecules* **1991**, *24*, 6803–6805.
- (23) Xi, H.; Milner, S. T. Bicontinuous Phase in Diblock Copolymer Melts with Added Homopolymer. *Macromolecules* **1996**, *29* (7), 2404–2411.
- (24) Gobius du Sart, G.; Vukovic, I.; Vukovic, Z.; Polushkin, E.; Hiekkataipale, P.; Ruokolainen, J.; Loos, K.; ten Brinke, G. Nanoporous Network Channels from Self-Assembled Triblock Copolymer Supramolecules. *Macromol. Rapid Commun.* **2011**, *32*, 366–370.
- (25) Nandan, B.; Vyas, M. K.; Böhme, M.; Stamm, M. Composition-Dependent Morphological Transitions and Pathways in Switching of Fine Structure in Thin Films of Block Copolymer Supramolecular Assemblies. *Macromolecules* **2010**, *43*, 2463–2473.
- (26) Ikkala, O.; ten Brinke, G. Functional Materials Based on Self-Assembly of Polymeric Supramolecules. *Science* **2002**, *295*, 2407–2409.
- (27) Mäki-Ontto, R.; de Moel, K.; de Odorico, W.; Ruokolainen, J.; Stamm, M.; ten Brinke, G.; Ikkala, O. "Hair Tubes": Mesoporous Materials Containing Hollow Self-Organized Cylinders with Polymer Brushes at the Walls. *Adv. Mater.* **2001**, *13*, 117–121.
- (28) Hillmyer, M. A. Nanoporous Materials from Block Copolymer Precursors. *Adv. Polym. Sci.* **2005**, *190*, 137–181.
- (29) Crossland, E. J. W.; Ludwigs, S.; Hillmyer, M. A.; Steiner, U. Control of Gyroid Forming Block Copolymer Templates: Effects of an Electric Field and Surface Topography. *Soft Matter* **2010**, *6*, 670–676.
- (30) Urade, V. N.; Wei, T. C.; Tate, M. P.; Kowalski, J. D.; Hillhouse, H. W. Nanofabrication of Double-Gyroid Thin Films. *Chem. Mater.* **2007**, *19*, 768–777.
- (31) Vukovic, I.; Punzhin, S.; Vukovic, Z.; Onck, P.; De Hosson, J.; Th., M.; ten Brinke, G.; Loos, K. Supramolecular Route to Well-Ordered Metal Nanofoams. *ACS Nano* **2011**, *5* (8), 6339–6348.
- (32) Valkama, S.; Ruotsalainen, T.; Nykänen, A.; Laiho, A.; Kosonen, H.; ten Brinke, G.; Ikkala, O.; Ruokolainen, J. Self-Assembled Structures in Diblock Copolymers with Hydrogen-Bonded Amphiphilic Plasticizing Compounds. *Macromolecules* **2006**, *39*, 9327–9336.
- (33) Borsboom, M.; Bras, W.; Cerjak, I.; Detollenaere, D.; Glastra van Loon, D.; Goedtkindt, P.; Konijnenburg, M.; Lassing, P.; Kevine, Y. K.; Munneke, B.; Oversluizen, M.; van Tol, R.; Vlieg, E. The Dutch–Belgian Beamline at the ESRF. *J. Synchrotron Radiat.* **1998**, *5*, 518–520.
- (34) Bras, W.; Dolbnya, I. P.; Detollenaere, D.; van Tol, R.; Malfois, M.; Greaves, G. N.; Ryan, A. J.; Heeley, E. Recent Experiments on a Combined Small-Angle/Wide-Angle X-ray Scattering Beam Line at the ESRF. *J. Appl. Crystallogr.* **2003**, *36*, 791–794.
- (35) Available at <https://secure.msri.org/about/sgp/jim/software/temsim/index.html>.
- (36) Ruokolainen, J.; Torkkeli, M.; Serimaa, R.; Komanschek, B. E.; Ikkala, O.; ten Brinke, G. Order–Disorder Transitions in Polymer–Surfactant Systems. *Phys. Rev. E* **1996**, *54*, 6646–6649.
- (37) Angerman, H. J.; ten Brinke, G. Weak Segregation Theory of Microphase Separation in Associating Binary Homopolymer Blends. *Macromolecules* **1999**, *32*, 6813–6820.
- (38) Feng, E. H.; Lee, W. B.; Fredrickson, G. H. Supramolecular Diblock Copolymers: A Field–Theoretic Model and Mean–Field Solution. *Macromolecules* **2007**, *40*, 693–702.
- (39) Hamley, I. W.; Castelletto, V. Small-Angle Scattering of Block Copolymers in the Melt, Solution and Crystal States. *Prog. Polym. Sci.* **2004**, *29*, 909–948.
- (40) Alberda van Ekenstein, G. O. R.; Meyboom, R.; ten Brinke, G.; Ikkala, O. Determination of the Flory–Huggins Interaction Parameter

of Styrene and 4-Vinylpyridine Using Copolymer Blends of Poly(styrene-co-4-vinylpyridine) and Polystyrene. *Macromolecules* **2000**, *33*, 3752–3756.

(41) Zha, W.; Han, C. D.; Lee, D. H.; Han, S. H.; Kim, J. K.; Kang, J. H.; Park, C. Origin of the Difference in Order-Disorder Transition Temperature between Polystyrene-block-poly(2-vinylpyridine) and Polystyrene-block-poly(4-vinylpyridine) Copolymers. *Macromolecules* **2007**, *40*, 2109–2119.